Focal mechanisms of small earthquakes in the southeastern Brazilian shield: a test of stress models of the South American plate

Marcelo Assumpção

Department of Geophysics, IAG, University of São Paulo, PO Box 3386, *São Paulo, SP,* 01060, *Brazil. E-mail: marcelo@iag.usp.br*

SUMMARY
Focal mechanisms of small earthquakes with magnitudes of about 3 in the SE Brazilian shield are calculated using S/P amplitude ratios. Low attenuation (Q_p from 400 to 800) in the shield upper-crustal layers allowed sharp S arrivals to be recorded up to distances of 100 km. Besides P-wave polarities, SH-wave first motions were also used to constrain the nodal-plane orientations. Normal and reverse faulting mechanisms with strike-slip components were found. The inversion of four mechanisms to estimate the stress tensor indicated a strike-slip stress regime with roughly E–W-orientated σ_1 and N–S σ_3. Both the orientations and the shape factor ($\varphi = 0.7$) of the inverted stress are in excellent agreement with theoretical predictions for that part of Brazil from the driving-force model of Coblentz & Richardson (1996). Good agreement with the nature of the stress, as well as its orientation, was also found for the model of Meijer (1995). Both of these theoretical models include spreading stresses along the continent/ocean lithospheric transition. Because the earthquakes are more than 300 km from the continental shelf they should not be affected by the local flexural forces caused by sediment load in the marginal basins. The agreement between observed and theoretical stresses then confirms the importance of continental spreading forces in modelling intraplate stresses.

Key words: fault-plane solutions, intraplate stresses, SE Brazil.

1 INTRODUCTION

What causes the motion of the South American plate? Is it 'pushed' by 'ridge push' and resisted by the asthenosphere, or is it passively carried by upper-mantle flow? Despite extensive modelling of the driving forces in the South American plate (Mendiguren & Richter 1978; Richardson *et al.* 1979; Stefanick & Jurdy 1992; Meijer & Wortel 1992; Meijer 1995; Coblentz & Richardson 1996) these questions do not yet have definite answers. The plate-driving forces can only be estimated indirectly by studying the stresses they cause in the plate interior. However, there are two difficulties with this approach: first, very few reliable stress measurements are available for the intraplate area of South America (Assumpção 1992; Lima *et al.* 1997) to define the observed lithospheric stress field, and second, local sources of stress can significantly perturb the regional field and should be taken into account when comparing the observed stresses with those due to the plate-driving forces.

Ridge push is known to be a major source of intraplate stress and is one of the main parameters in theoretical models of the South American plate. Ridge push arises from the imbalance of the vertical density distribution in the cooling oceanic lithosphere, which causes lithospheric compressional stresses under the deep oceanic basins. Because the density structure of the cooling oceanic lithosphere is fairly well known, ridge push can be estimated reasonably well. The nature of the shear stresses in the lithosphere/asthenosphere boundary, on the other hand, depends on the upper-mantle flow pattern, which is not known in detail. Preliminary estimates of the basal shear from models of global circulation driven by heterogeneities defined by seismic tomography are still much affected by uncertainties in physical parameters of the upper mantle (Bai *et al.* 1992). If the basal shear helps the westward plate motion then upper-mantle flow could be the main driving mechanism for the South American plate; if the basal shear resists the plate motion, then the movement of the lithospheric plate is controlled by other forces and could be independent of flow in the asthenosphere and lower mantle. The basal shear can be estimated indirectly by theoretical modelling of the resulting intraplate stresses, but is not well constrained with the present stress data (Meijer 1995).

Recent force models of the South American plate (Meijer 1995; Coblentz & Richardson 1996) have reproduced the main first-order patterns of lithospheric stress. These models have also shown that large-scale lateral variations of topography and plate structure (such as in the continent/ocean transition) can have a profound effect on the intraplate stresses. Lima

et al. (1997) analysed borehole breakout data in several Brazilian sedimentary basins and showed that in the equatorial margin and in central Brazil the first-order stress models (Meijer 1995; Coblentz & Richardson 1996) are generally consistent with the few available stress data, but local flexural stresses near the continental shelf are more important that the regional plate-wide stresses. Nevertheless, it is interesting to observe that the preferred theoretical models of Meijer (1995) and Coblentz & Richardson (1996) include a small driving basal shear.

To constrain further the theoretical force models, however, better data coverage of the intraplate stress field is necessary because most stress data in South America are concentrated in the Andean region (Assumpção 1992; Lima *et al.* 1997). Also, in the continental area, far from plate-boundary perturbations, most available stress data are single focal mechanism solutions. The purpose of this paper is to determine additional focal mechanisms of small events in the SE Brazilian shield (events 1–4 in Fig. 1), far from the local perturbations of the continental margin, and compare the stress tensor obtained from these mechanisms with the stresses inferred from theoretical force models. It will be shown that the observed stress tensor is in very good agreement with the directions and types of stresses inferred from the theoretical models.

2 DETERMINATION OF FOCAL MECHANISM USING S/P AMPLITUDE RATIOS

For small events recorded by few local stations, P- and S-wave first motions are not usually enough to constrain the focal mechanism. The information contained in the amplitude ratios of P and S waves can then be very helpful to restrain the number of possible nodal-plane solutions (e.g. Kisslinger 1980; Kisslinger *et al.* 1982).

Both the SV/SH ratio (i.e. the S-wave polarization) and the SH/P ratio were used to search all fault-plane parameters (dip, strike and slip) in steps of 5° and select the solutions that satisfy the polarity data and that fit the amplitude ratios within a given maximum residual in terms of log(amplitude ratio). We used the code FOCMEC, developed by Snoke *et al.* (1984). No errors were allowed in the P and SH polarities because only clear first motions were used.

The observed amplitudes were corrected for the free-surface effect. With three-component digital stations, the P-wave particle motion was used to obtain the arriving emergence angles at the surface. Emergence angles for the S waves were assumed to be the same as for the P arrivals and were usually shallower than the shear-wave window.

S-wave polarization and SV/SH ratio

For shallow emergence angles, the S-wave particle motion is non-linear and a direct measurement of the polarization angle is not usually possible. However, the use of the absolute amplitudes of the vertical and transverse components (which is related to the polarization angle) helps reduce the range of possible fault-plane solutions.

The SV amplitude was measured in the vertical component because it is much less disturbed by near-surface effects than the radial component (Booth & Crampin 1985). Large S to P conversions, especially in the case of spherical wave fronts and low-velocity layers near the surface, can significantly perturb the radial component of the S wave recorded at the surface. Despite the difficulties of measuring S amplitudes arriving at shallow angles, even a rough estimate of the SV amplitude (to
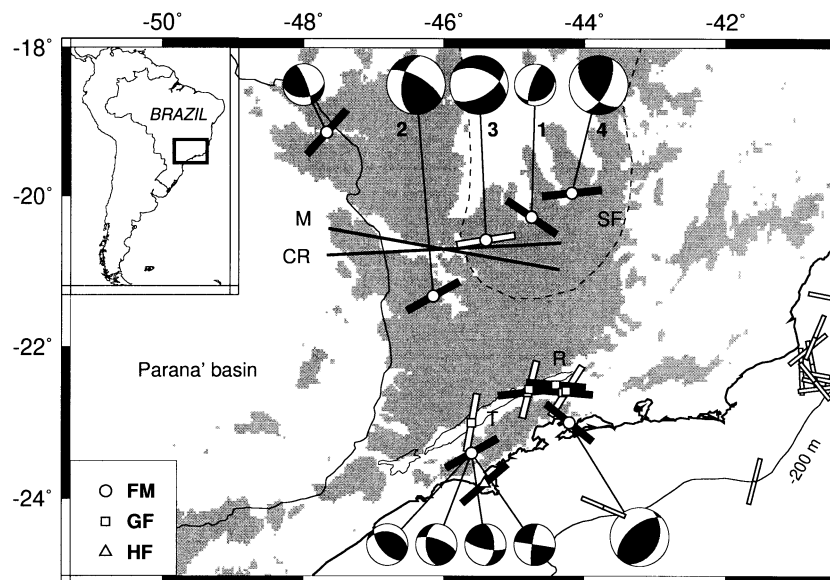

Figure 1. Location map and nodal-plane solutions of events 1–4 shown in Table 1. Short, thick bars indicate estimates of the $SH_{\max}$ orientation: solid bars = P-axes for reverse or strike-slip events (approximately σ_1); and open bars = B-axes for the normal faulting events. Data from focal mechanism (FM), slickenside inversion of Quaternary geological faults (GF), and hydraulic fracturing (HF, Cláudio Lima, personal communication, 1996). Breakout data offshore (thin open bars) from Lima *et al.* (1997). Lines labelled M and CR indicate the $SH_{\max}$ orientations calculated by thin-shell, finite-element modelling of the South American plate by Meijer (1995) and Coblentz & Richardson (1996), respectively. Other focal mechanisms from Mendiguren (1980), Berrocal *et al.* (1993) and Assumpção *et al.* (1997). The grey shade indicates elevations higher than 800 m. The solid line in the continent indicates the limits of the Palaeozoic intracratonic Paraná basin, and the dashed line indicates the limits of the São Francisco craton (SF). Thin lines indicate the Taubaté (T) and Rezende (R) Tertiary basins in the Paraíba graben.

within a factor of 2 or more) is extremely useful in constraining the nodal-plane solution together with a few other polarity data (Kisslinger 1980; Kisslinger *et al.* 1982).

SH/P amplitude ratio

We also used the *SH/P* amplitude ratio to help constrain the focal mechanism. Because epicentral distances up to about 100 km were used, it was necessary to correct the amplitudes for anelastic attenuation. Average *Q* values, for both *P* and *SH* waves, were estimated using the method of Al-Shukri & Mitchell (1990) and Hough *et al.* (1988) based on the model of f^{-2} decay of the source displacement spectrum. In this case, the high-frequency slope of the acceleration spectra is directly proportional to Q^{-1}. As an example, Fig. 2 shows the acceleration spectra for the Formiga event (magnitude 2.5, event 3 in Table 1) recorded at a distance of 27 km. A magnitude 2.5 *mb* is expected to have a corner frequency of about 3–5 Hz (Nuttli 1983). In Fig. 2 the slopes were measured in the range 10–80 Hz for the *P* arrival and 5–40 Hz for the *S* arrival, giving values of $Q_p = 400$ and $Q_s = 1000$, respectively. Measurements of Q_p for other event–station pairs were mostly in the range 400–800, and Q_s ranged from about 500 to 2000, with an average Q_s/Q_p ratio of about 1.7. Values of Q_s higher than Q_p have been found in other studies of upper-crustal attenuation using local events such as discussed by Hough & Anderson (1988). The high values of *Q* found for the upper crust in this shield area
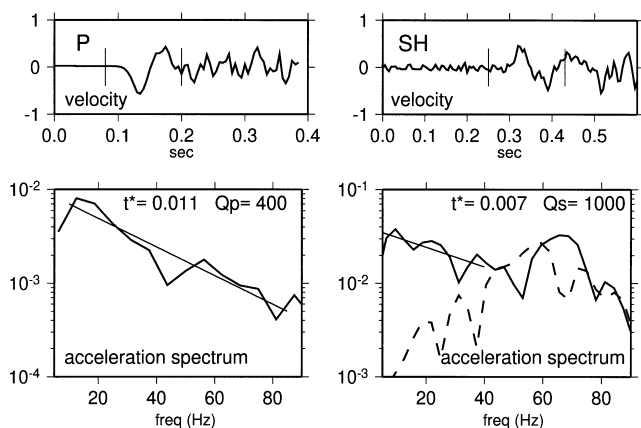
explain why clear *P-* and *S*-wave first motions from small events with magnitude ≈ 2 can be observed at distances up to 100 km.

Corrections of the amplitude ratios *SH/P* were usually less than 30 per cent. For distances greater than 100 km, the uncertainties in the *Q* estimates are higher, mainly because the acceleration spectra show less stable slopes due to noise contamination at the high-frequency end. For this reason no amplitude ratios were used beyond 100 km.

2.1 The Formiga event of 1993 September 29 (#3 in Table 1)

Fig. 3 shows the Formiga epicentre and the four digital stations (27–184 km distant) used to determine the focal mechanism. For stations FRMB and CDCB, as well as *P* and *SH* polarities, *SV/SH* and *SH/P* amplitude ratios were used. For station FURB, at a distance of 92 km, only the *SH/P* amplitude ratio was used. At CACB no amplitude information was used and only the dilatational *P* polarity helped constrain the nodal-plane solution. Fig. 4 shows all possible solutions with a maximum residual of 0.30 in all but one station (that is one error was allowed in the five amplitude ratios used). Table 2 shows the resulting amplitude ratios for the best solution. The best solution has a rms in the log(amplitude ratio) of 0.09 for the four stations that satisfied the 0.30 limit, and a rms of 0.23 with all five stations used. The solutions in Fig. 4 show a predominantly normal faulting event with a N–S-orientated T axis.
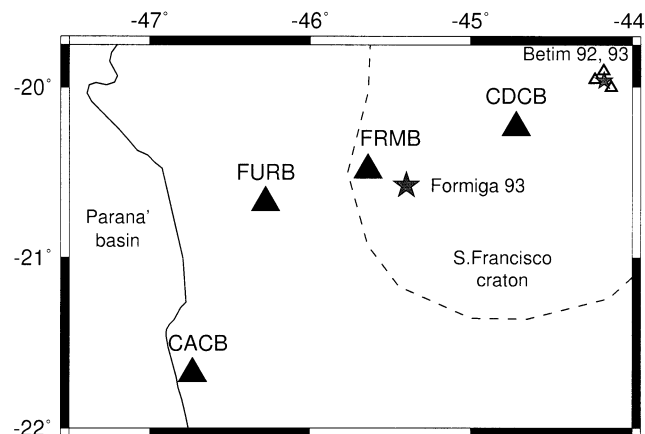

Figure 2. Example of *Q* determination using the first cycle of the direct *P* (right) and *S* (left) waves of the 2.5 *mb* Formiga event (# 3) recorded at FRMB at a distance of 27 km. Thin vertical lines in the top traces indicate the windows for the acceleration spectra shown below. The high-frequency slope of the acceleration spectra is related to the effective *Q* along the path. The dashed line in the lower-right diagram refers to the noise spectrum before the direct *S* arrival. Spectral noise before the *P* arrival is below the limits of the figure.

Figure 3. Epicentres of the Formiga 1993 and Betim 1992/93 events (3 and 4 in Table 1, respectively). Large solid triangles are the digital stations that recorded the Formiga event; small open triangles are local analogue stations that recorded the Betim 1992 series. The Betim event (October 1993) was recorded by the digital station CDCB.
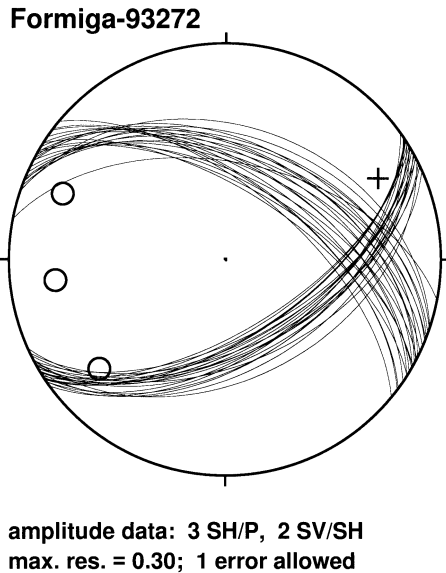
Table 1. Epicentral data and focal-mechanism solutions. Event numbers as in Fig. 1.

#	Locality	Date yyyy/mm/dd	Lat. (°S)	Long. (°W)	Depth (km)	Mag.	Focal mechanism strike	dip	slip	Reference
1	Cajuru	1976	−20.26	−44.75	1	<3.2	70	24	138	Viotti *et al.* 1997
2	Areado	1991/10	−21.33	−46.15	1.5	<2.0	190	50	151	Blum 1993
3	Formiga	1993/09/29	−20.58	−45.40	0	2.5	292	48	−48	this paper
4a	Betim	1992/08	−19.96	−44.18	3	1.0	136	50	35	this paper
4b	Betim	1993/10/08	−19.96	−44.18	3	2.6	146	56	53	this paper
4c	Betim	composite	−19.96	−44.18	3	—	138	55	35	this paper

Formiga-93272

amplitude data: 3 SH/P, 2 SV/SH
max. res. = 0.30; 1 error allowed

Figure 4. Possible nodal-plane solutions for the Formiga event satisfying all the polarity data and all but one of the log(amplitude ratios). Maximum log(amplitude ratio) allowed is 0.30. Circles and cross denote *P*-wave dilatational and compressional first motions, respectively.
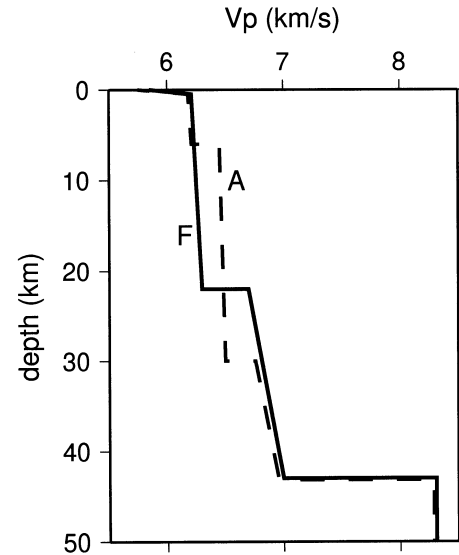

Figure 5. Two crustal velocity models used with the Formiga event: F is the preferred regional model as determined by Assumpção (1994); A is a perturbation of F to test the stability of the nodal-plane solution.

Table 2. Amplitude ratios for the Formiga 1993 best nodal-plane solution. Strike = 292, dip = 48, slip = −48. (Using $Q_s = 1.7 Q_p$.)

Station	Distance (km)	Azimuth (°)	Amplitude ratio	Log(amplitude ratio) obs.	theor.	residue	Q_p
FRMB	26.7	292	*SH/P*	+0.64	+0.82	−0.18	400
			SV/*SH*	+0.11	+0.06	+0.05	
CDCB	80.6	62	*SH/P*	+1.33	+1.24	+0.09	400
			SV/SH	−1.31	−0.97	−0.34	
FURB	92.0	263	*SH/P*	−0.08	−0.11	+0.03	800

The hypocentre determination for this event indicated very shallow depths: 0 km was obtained when using the crustal velocity model derived by Assumpção (1994) for this region (Fig. 5). Because the nearest station was 26 km away, the actual depth is not very well constrained. To investigate the stability of the nodal-plane solutions two different crustal models ('F' and 'A' in Fig. 6) and three different depths were tried. The take-off angles at the source will vary, depending on the depth and velocity model, which will affect the focal mechanism solution. Fig. 6 shows the best solutions for each case: the two numbers on the upper left of each diagram are the amplitude ratio rms, the first for the stations that satisfied the error limit, and the second (in parentheses) for all stations. As the depth is increased the solution gets worse. This is consistent with the preferred hypocentral depth of 0 km determined by the regional velocity model.

2.2 The Betim series of 1992 and 1993 (#4 in Table 1)

In June 1992 a series of small earthquakes started in the town of Betim, many of which were felt by the population. Local stations were installed in the area from July 15 (analogue, vertical-component seismographs), as shown in Fig. 3. The largest event (1992 July 25) had a magnitude of 2.8 and caused intensities up to V–VI MM. Several events were recorded by the local temporary stations as well as a few other regional stations. All events showed exactly the same *P*-wave polarity and *P/S* amplitude patterns at each of the three local stations, indicating that they all had the same hypocentre and focal mechanism. The activity decreased at the end of 1992 and early 1993, and only one local station remained in operation. The average *SV/P* amplitude ratios of the two best-recorded events (August 17 and 29) were used to determine the nodal-plane solutions, allowing a maximum error in the log(ratio) of 0.30 (Fig. 7a). The solutions indicate strike-slip faulting with a reverse component.

On 1993 August 1 and October 8, two other events (magnitudes 2.4 and 2.6) from Betim were recorded with identical waveforms by a few regional digital stations. Both instrumental data and macroseismic information indicate that the 1992 and 1993 epicentres were very close. Also, the *P* and *SH* first-motion directions at CDCB are consistent with the best solutions of the 1992 events. Assuming the 1993 events had the same mechanism as the 1992 series, we determined the nodal-plane solutions for the 1993 largest event using the *SV/SH* and the *SH/P* amplitude ratios at CDCB with additional *P*-wave polarities from the 1992 series. These solutions (Fig. 7b) show predominantly reverse faulting with a strike-slip component, very similar to the 1992 solutions (see Table 1). The similarity of the two sets of solutions and low
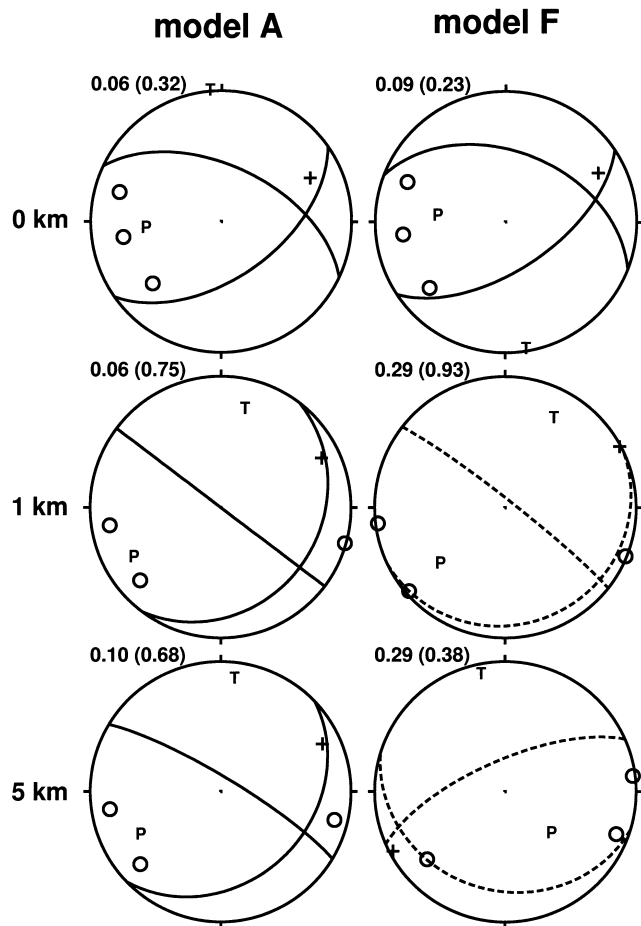
model A   model F

Figure 6. The best nodal-plane solutions for models A and F at three different hypocentral depths (0, 1 and 5 km). The numbers on the upper left side of each diagram are the rms residues of the log(ratio): the first refers to the four amplitude data within the error limit of 0.3, and the second (in parentheses) is the rms for all five data values.

residuals in the amplitude ratios allow the determination of a composite solution combining all polarity and amplitude ratios, as carried out in Fig. 7(c). The results of the best-fitting composite solution are given in Table 3.

3 OTHER FOCAL MECHANISMS

3.1 Cajuru (#1 in Table 1 and Fig. 1)

A series of reservoir-induced earthquakes have been observed near the Cajuru dam since 1970 with magnitudes up to 3.7 and intensities up to V–VI. Although the activity decreased sharply after 1978, some small earthquakes were still recorded by the local stations up to 1995 (Viotti *et al.* 1997). A composite focal mechanism, determined with a seven-station network deployed in the reservoir area during July/August 1976 (Mendiguren & Richter 1978; Viotti *et al.* 1997), shows reverse faulting. This composite solution has several inconsistencies, indicating that focal mechanisms may vary somewhat across the seismic area, which does not seem to be restricted to a single fault but is spread in an area about 4 km across (Viotti *et al.* 1997). However, a 2.5 *mb* event in December 1993, recorded by the digital station CDCB installed in the reservoir
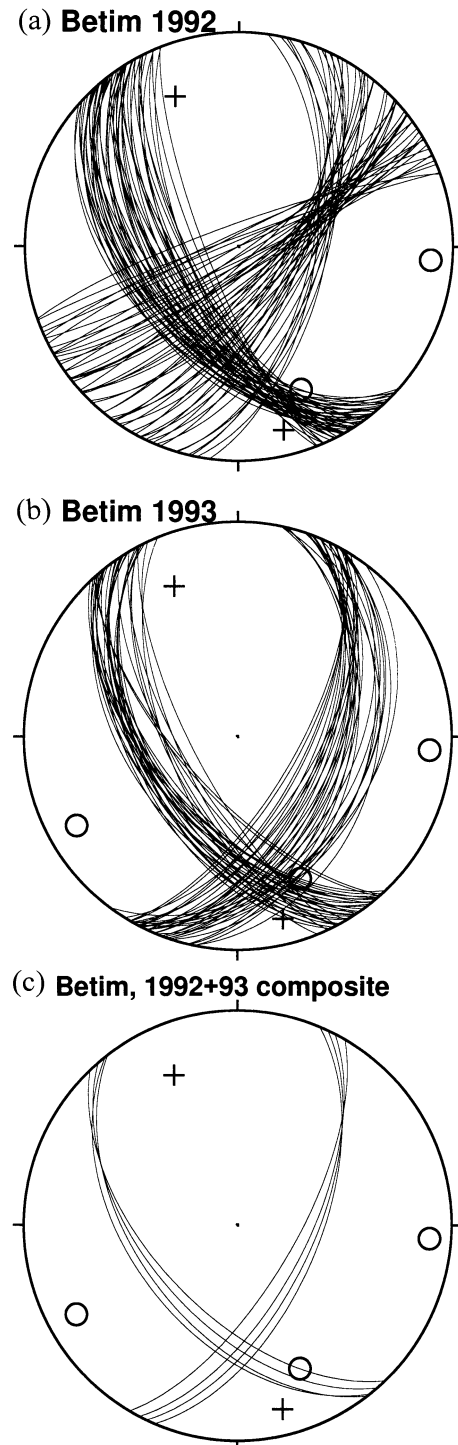

Figure 7. Nodal-plane solutions of the Betim events, assuming that the 1992 and 1993 swarms had the same mechanism. A maximum residual of 0.3 was set for the log (amplitude ratios) with no errors allowed. (a) Solutions for the 1992 event using only data from the local stations (BET1, 2 and 3) and an additional *P*-wave first motion from a regional station. (b) Solutions using the amplitude data (*SV/SH* and *SH/P*) of the 1993 event at station CDCB, together with the *P*-wave first motions of the 1992 swarm. (c) Composite solutions using all data from (a) and (b).

Table 3. Amplitude ratios for the composite Betim 1992–1993 best nodal-plane solution. Strike = 138°, dip = 55°, slip = 35.

Station	Distance (km)	Azimuth (°)	Amplitude ratio	Log(amplitude ratio) obs.	theor.	res.
BET1	3.5	157	*SV/P*	+0.45	+0.34	+0.11
BET2	7.2	274	*SV/P*	−0.42	−0.31	−0.11
BET3	6.3	346	*SV/P*	+1.06	+0.92	+0.14
CDCB	65.7	241	*SH/P*	+0.18	+0.35	−0.17
CDCB			*SV/SH*	−0.30	−0.17	−0.14

area, had *P*- and *SH*-wave polarities as well as *P/SV/SH* amplitude ratios consistent with the early composite solution of the 1976 studies. The epicentre, 4.5 km from the station, was also in the middle of the active area determined by the early studies (Assumpção *et al.* 1997).

3.2 Areado 1991 (#2 in Table 1 and Fig. 1)

A swarm of small earthquakes started in the town of Areado in September 1991. The largest events reached magnitude 3 and intensities IV MM. A local five-station network deployed in October 1991 recorded tens of events (Blum 1993), and showed that the activity was concentrated in an area less than about 2 km across. A well-constrained nodal-plane solution, with almost no inconsistent polarities, was obtained with the local stations indicating a predominantly reverse faulting mechanism. The two largest events of the Areado swarm had *P*-wave first motions recorded at three other regional stations, from 70 to 230 km away, which were also consistent with the focal mechanism determined with the local stations (Assumpção *et al.* 1997). The distribution of hypocentres favours the NW-dipping, SSW-striking plane to be the rupture plane (Blum 1993).

4 OBSERVED STRESSES AND MODEL PREDICTIONS

4.1 Observed stresses

Fig. 1 shows the available focal mechanisms in the SE Brazilian shield. Besides the events # 1–4 (Table 1), other mechanisms and stress indicators near the continental margin are also shown. A rough estimate of the observed maximum horizontal stress (SH_{max}) can be taken from the directions of the P-axes of reverse or strike-slip mechanisms, and the B-axes of normal faulting mechanisms (shown as short bars with a circle in Fig. 1). Although the P- and T- axes of earthquake mechanisms are not exactly the principal stress directions, they are useful first-order approximations to the tectonic stress regime (Assumpção 1992; Zoback 1992). Away from the continental margin, the observed estimated SH_{max} orientations show a uniform pattern with an ENE–WSW average direction. Near the coast the data are more scattered.

Near the coast, strike-slip and reverse faulting mechanisms are found. One shallow (60–80 m deep) hydraulic fracturing measurement indicated a coast-parallel compressional stress (Cláudio Lima, personal communication, 1996) consistent with the maximum horizontal stress inferred from the nearby focal mechanisms. In the Paraiba graben (near the Taubaté and Rezende basins, Fig. 1), inversion of striae from recent geological faults indicates variable stress regimes with normal, strike-

slip and reverse faulting observed. Although very recent geological faults were found (Pleistocene to Holocene), the stresses associated with them seem to vary with time (Riccomini *et al.* 1989; Salvador & Riccomini 1995): NW–SE compression in the Pleistocene followed by WNW–ESE extension in the middle Holocene, and E–W compression at present. It is not clear whether the normal faulting represents real changes of the lithospheric stress regime or just secondary, surface effects of a more uniform, regional deformation.

Further from the continental margin, however, the observed SH_{max} orientations (estimated from the focal mechanisms) are more uniform, and correlate well with the directions predicted by the theoretical models of Meijer (1995) and Coblentz & Richardson (1996), labelled M and CR in Fig. 1. The mixture of reverse, strike-slip and normal faulting suggests that the crustal stress regime is strike-slip, in agreement with the theoretical models, as shown below.

4.2 Stress inversion from focal mechanisms

Different focal mechanisms in the same area can result from different orientations of pre-existing fault planes under the same uniform crustal stress field. Inversion of the focal mechanisms to obtain the principal directions of the crustal stress can then be carried out if the assumption of a uniform stress field is valid. In order to make a better comparison between the observed focal mechanisms and the theoretical predictions, we inverted the four nodal-plane solutions of Table 1 by minimizing the difference between the slip direction and the shear stress direction in the fault plane. A grid search was carried out to find the directions of the three principal stresses (σ_1, σ_2 and σ_3) and the shape factor $\varphi = (\sigma_2 - \sigma_3)/(\sigma_1 - \sigma_3)$, σ_1 and σ_3 being the most and the least compressional stresses, respectively. This method assumes that the slip direction of the earthquake rupture is given by the ambient shear stress in the fault plane, which is usually thought to be a valid assumption. The mismatch between slip and shear directions in the fault plane can be due to either a non-uniform stress field, or errors in the fault-plane solution. The focal mechanisms shown in Table 1 do not distinguish which of the nodal planes is the actual fault plane. In this case, at every step of the grid search for the stress tensor, the nodal plane with the least mismatch angle is chosen. A code by Michael (1987) was used for the grid search with steps of 5° in the stress directions and 0.1 in the shape factor. Because only four earthquakes were available, a finer grid was not thought to be justifiable.

Fig. 8 shows all four fault planes with the mismatch between the slip directions, given by the focal mechanisms (arrows), and the shear stress direction in the fault plane. The average mismatch angle is only 3°. The grid-search inversion predicted the right fault plane for the event of Areado (#2), which was
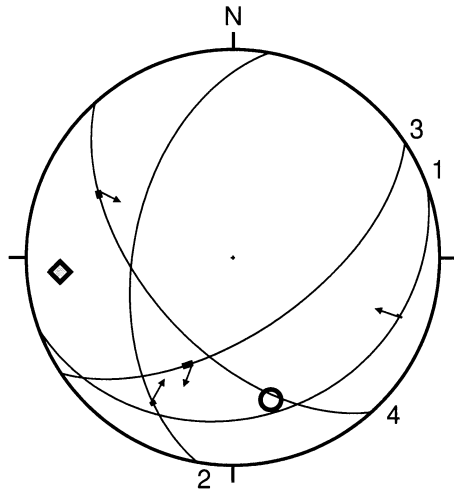
Figure 8. Inversion of the four focal mechanisms. Labels 1–4 indicate the assumed fault plane for the four events of Table 1. The thick segment in the fault plane shows the difference between the calculated shear stress and the observed slip vector. The arrows indicate the observed slip vector: inward arrows denote reverse components, outward arrow a normal component. The diamond and the open circle indicate the principal stresses, σ_1 and σ_3, respectively (see Table 4).

the only event with a known fault plane. The inversion result (Table 4 and Fig. 8) shows a strike-slip stress regime with σ_1 nearly E–W and σ_3 N–S, and a shape factor of $\varphi = 0.7$, in good agreement with the predictions of Coblentz & Richardson (1996).

4.3 Stress models of the South American plate

Comparisons of the observed stress directions with predictions from finite-element models of the South American plate have been used to study the plate-driving forces. Calculations that only use plate-boundary forces (such as ridge push, collision with the Nazca plate and a balancing asthenospheric drag) predict slowly varying, compressional stresses in the plate interior (Richardson *et al.* 1979; Stefanick & Jurdy 1992; Meijer 1995; Coblentz & Richardson 1996). Recent, more detailed stress models of the South American plate including internal spreading stresses due to large-scale lateral density contrasts along the continent/ocean transition have been proposed (Meijer 1995, his Fig. 3.37, and Coblentz & Richardson 1996, their model 3). We call these two models M and CR, respectively. The lateral density contrast between continental/oceanic lithosphere causes extensional stresses in the continent and compressional stresses in the ocean (e.g. Bott & Dean 1972). These so-called 'spreading stresses' at the continental margin were incorporated in the theoretical finite-element models M
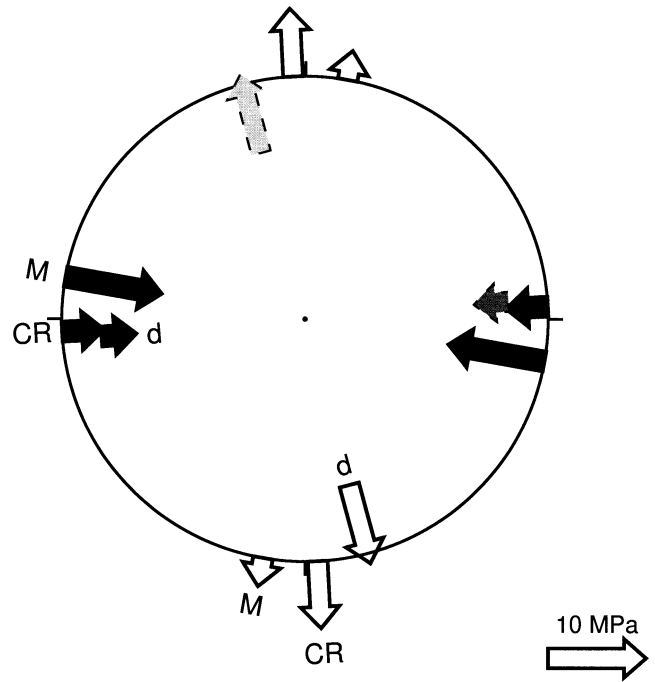

Figure 9. Principal stresses in SE Brazil (σ_1 and σ_3, inward and outward arrows, respectively) from two theoretical force models of the South American plate ('M' = Meijer 1995; 'CR' = Coblentz & Richardson 1996), compared with results from the inversion of four focal mechanisms ('d'). Arrow sizes scaled according to Table 4. Equal-area projection: solid and open arrows refer to lower hemisphere, grey arrows to upper hemisphere.

and CR by using body forces pulling the continent towards the ocean. Thin-shell, finite-element calculations with a 100 km thick elastic lithosphere were used in both models, predicting compressional stresses in the oceanic lithosphere (of the order of 20–30 MPa) and strike-slip stresses in the continental part of the plate. The magnitude of the differential stresses ($\sigma_1 - \sigma_3$) in the continent decreases from about 20 MPa in northern Brazil to about 5–10 MPa in southern Brazil. Models that incorporate the spreading stresses at the continental margin match the observed stress patterns better than more simple force models.

Besides comparing the theoretical and observed directions of the principal stresses, the relative stress magnitudes are also shown in Fig. 9. It is not usually possible to obtain absolute values of the stresses (either total or deviatoric stresses) from inversion of earthquake mechanisms. In Table 4, the values of σ_1 and σ_3 of models M and CR are the 'tectonic' stresses, that is the differences between the total principal stresses and the lithostatic stress (in this case the lithostatic stress is σ_2, and its

Table 4. Theoretical and observed principal stresses in SE Brazil.

	Magnitudes (MPa)[+]		φ	Azimuth/Plunge[*]		Reference
	σ_1	σ_3		σ_1	σ_3	
M	+10	−3	0.2	280/0	190/0	Meijer (1995)
CR	+4	−7	0.6	267/0	177/0	Coblentz & Richardson (1996)
data	—	—	0.7	265/17	165/30	inversion of four focal mechanisms

[+] Magnitudes in excess of the lithostatic pressure
[*] In the thin-shell theoretical models M and CR, the principal stress directions are necessarily horizontal and vertical

'tectonic' component, by definition, will be zero). The stress difference ($\sigma_1-\sigma_3$) is very similar in both models and averages about 12 MPa. For the sake of comparison, in Fig. 9 the sizes of the arrows of the inverted stresses were scaled by normalizing the stress difference ($\sigma_1-\sigma_3$) to 12 MPa. The relative sizes of the σ_1 and σ_3 arrows will then indicate the shape factor φ. It is clear that the observed stress (labelled 'd' in Fig. 9) is very similar to the theoretical model of Coblentz & Richardson (1996).

The complex stress pattern near the continental margin (Fig. 1), on the other hand, is more difficult to compare with theoretical models because of the local sources of stress arising at the continent/ocean transition. First, due to the size of the finite-element cells, it is not expected that theoretical models, such as M and CR, will have enough resolution to predict detailed stress patterns near the continental margin, thus a comparison with observations too near the coast is not warranted. Second, local flexural stresses from the sediment load in the continental shelf and erosion at the continental margin, not taken into account in the theoretical models M and CR, are also important and are believed to affect the stresses up to a few hundred kilometres inland (e.g. Stein *et al.* 1989; Lima *et al.* 1997). In addition, the temporal variations of the observed stresses near the margin, as discussed previously, may also reflect the ongoing evolution of the coastal topography and the Paraíba graben.

We conclude that the thin-shell, finite-element models of the South American plate (M and CR), which take into account the large-scale spreading stresses at the continental margin, do predict the right kind of crustal stress pattern in the SE Brazilian shield away from the local flexural disturbances of the continental margin. Other force models that do not incorporate spreading stresses at the continental margin predict a purely compressional stress regime throughout the continental area (Stefanick & Jurdy 1992; Meijer 1995; Coblentz & Richardson 1996). Because the observed earthquakes are about 400–500 km from the continental/oceanic crustal transition, the spreading stresses caused by the lateral density contrasts between continental and oceanic lithospheres in South America can affect the intracontinental stress field up to at least 400 km inland.

Although model CR better matches the observed stresses in SE Brazil (Fig. 9), this does not imply that it is a better overall model of the driving forces in the South American plate. In fact, in NE Brazil, earthquake focal mechanisms and borehole breakout data are in better agreement with model M than model CR (Lima *et al.* 1997; Ferreira *et al.* 1998). The average difference between the SH_{max} directions of the two models is only about 20°.

5 CONCLUSIONS

Determination of the forces that drive the plate motions requires a good knowledge of the observed intraplate stress field. On the other hand, few reliable lithospheric stress indicators are usually available in mid-plate, low-seismicity areas such as in the South American continent, far from plate-boundary perturbations or local anomalies caused by the continental shelf.

However, because of the low seismic attenuation (high Q values) in shield areas, small earthquakes (magnitude 2–3) can have sharp S-wave arrivals recorded up to a distance of about 100 km. This allows the use of S/P amplitude ratios for the determination of nodal-plane solutions, increasing the data set of intraplate stress indicators.

In the SE Brazilian shield, nodal-plane solutions of four small events, located more than 300 km from the shoreline, indicate both normal and reverse types of faulting with strike-slip components. These different mechanisms are consistent with a uniform strike-slip stress tensor with roughly E–W maximum horizontal compression and N–S minimum compression. This stress tensor is in excellent agreement with the average lithospheric stresses inferred from theoretical models of the forces driving the South American plate (Meijer 1995; Coblentz & Richardson 1996). Because the earthquakes are far from suspected local sources of stress, such as flexural forces at the continental shelf, they are probably a good test of the theoretical models.

REFERENCES

Al-Shukri, H.J. & Mitchell, B.J., 1990. Three-dimensional attenuation structure in and around the New Madrid seismic zone, *Bull. seism. Soc. Am.,* **80,** 615–632.

Assumpção, M., 1992. The regional intraplate stress field in South America, *J. geophys. Res.,* **97,** 11 889–11 903.

Assumpção, M., 1994. A preliminary crustal model for SE Brazilian shield based on local earthquakes in southern Minas Gerais, *I Regional seism. Assembly S. America, Brasília,* abstracts, 78.

Assumpção, M., Barbosa, J.R., Berrocal, J., Bassini, A.M., Veloso, J.A.V., Huelsen, M.G. & Ribotta, L.C., 1997. Recent seismicity in southern Minas Gerais state, *Rev. Bras. Geofís.,* **15,** 119–132.

Bai, W., Vigny, C., Ricard, Y. & Froidevaux, C., 1992. On the origin of deviatoric stresses in the lithosphere, *J. geophys. Res.,* **97,** 11 729–11 737.

Berrocal, J., Fernandes, C., Bueno, A., Seixas, N. & Bassini, A., 1993. Seismic activity in Monsuaba (state of Rio de Janeiro), Brazil, between 1988 December and 1989 February, *Geophys. J. Int.,* **113,** 73–82.

Blum, M.L.B., 1993. Cálculo de magnitudes, estimativa do parâmetro *b* e considerações sobre a atividade sísmica de Areado, MG, outubro de 1991, *Proc. III Int. Congr. Brazilian Geophys. Soc., Rio de Janeiro, 1993,* **1,** 694–699.

Booth, D.C. & Crampin, S., 1985. Shear-wave polarization on a curved wavefront at an isotropic free surface, *Geophys. J. R. astr. Soc.,* **83,** 31–45.

Bott, M.H.P. & Dean, D.S., 1972. Stress systems at young continental margins, *Nature Phys. Sci.,* **235,** 23–25.

Coblentz, D.D. & Richardson, R.M., 1996. Analysis of the South American intraplate stress field, *J. geophys. Res.,* **101,** 8643–8657.

Ferreira, J.M., Oliveira, R.T., Takeya, M.K. & Assumpção, M., 1998. Superposition of local and regional stresses in NE Brazil: evidence from focal mechanisms around the Potiguar marginal basin, *Geophys. J. Int.,* accepted.

Hough, S.E. & Anderson, J.G., 1988. High-frequency spectra observed at Anza, California: implications for Q structure, *Bull. seism. Soc. Am.,* **78,** 692–707.

Hough, S.E. *et al.* 1988. Attenuation near Anza, California, *Bull. seism. Soc. Am.,* **78,** 672–691.

Kisslinger, C., 1980. Evaluation of S to P amplitude ratios for determining focal mechanisms from regional network observations, *Bull. seism. Soc. Am.,* **70,** 999–1014.

Kisslinger, C., Bowman, J.R. & Koch, K., 1982. Determination of focal mechanism from SV/P amplitude ratios at small distances, *Phys. Earth planet. Inter.,* **30,** 172–176.

Lima, C., Nascimento, E. & Assumpção, M., 1997. Stress orientations in Brazilian sedimentary basins from breakout analysis—implications for force models in the South American plate, *Geophys. J. Int.,* **130,** 112–124.

Meijer, P.T., 1995. Dynamics of active continental margins: the Andes and the Aegean region, *PhD thesis,* Utrecht University, the Netherlands.

Meijer, P.T. & Wortel, M.J.R., 1992. The dynamics of motion of the South American plate, *J. geophys. Res.,* **97,** 11 915–11 931.

Mendiguren, J.A., 1980. A procedure to resolve areas of different source mechanisms when using the method of composite nodal plane solution, *Bull. seism. Soc. Am.,* **70,** 985–998.

Mendiguren, J.A. & Richter, F.M., 1978. On the origin of compressional intraplate stresses in South America, *Phys. Earth planet. Inter.,* **16,** 318–326.

Michael, A.J., 1987. Use of focal mechanisms to determine stress: a control. study, *J. geophys. Res.,* **92,** 357–368.

Nuttli, O.W., 1983. Average seismic source-parameter relations for mid-plate earthquakes, *Bull. seism. Soc. Am.,* **73,** 519–535.

Riccomini, C., Pellogia, A.U.G., Saloni, J.C.L., Kohnke, M.W. & Figueira, R.M., 1989. Neotectonic activity in the Serra do Mar rift system (SE Brazil), *J. S. Am. Earth Sci.,* **2,** 191–197.

Richardson, R.M., Solomon, S.C. & Sleep, N.H., 1979. Tectonic stress in the plates, *Rev. Geophys. Space Phys.,* **17,** 981–1019.

Salvador, E.D. & Riccomini, C., 1995. Neotectônica da região do alto estrutural de Queluz (SP-RJ, Brasil), *Rev. Bras. Geociências.,* **25,** 151–164.

Snoke, J.A., Munsey, J.W., Teague, A.G. & Bollinger, G.A., 1984. A program for focal mechanism determination by combined use of polarity and SV-P amplitude ratio data, *Earthq. Notes,* **55** (3), 15.

Stefanick, M. & Jurdy, D.M., 1992. Stress observations and driving forces models for the South American plate, *J. geophys. Res.,* **97,** 11 905–11 913.

Stein, S., Cloetingh, S., Sleep, N.H. & Wortel, R., 1989. Passive margin earthquakes, stresses and rheology, in Earthquakes at North-Atlantic Passive Margins: Neotectonics and Postglacial Rebound, pp. 231–259, eds Gregersen, S. & Basham, P.W., Kluwer, Dordrecht.

Tapley, W.C. & Tull, J.E., 1991. *SAC—Seismic Analysis Code,* Lawrence Livermore National Laboratory, CA.

Viotti, C.B., Veloso, J.A.V. & Gomide, L.C., 1997. Induced seismicity at Cajuru reservoir, Minas Gerais, Brazil, *Proc. Int. Congress Large Dams, Italy, 1997,* 1211–1225.

Wessel, P. & Smith, W.H.F., 1991. Free software helps map and display data, *EOS, Trans. Am. geophys. Un.,* **72,** 445–446.

Zoback, M.L., 1992. Stress field constraints on intraplate seismicity in Eastern North America, *J. geophys. Res.,* **97,** 11 761–11 782.